Revealing and characterising solidification structure of ductile cast iron

G. Rivera, R. Boeri, and J. Sikora

This study deals with the solidification and microsegregation processes of near eutectic ductile cast iron. A detailed analysis of old and new solidification models was made. Metallographic techniques, developed elsewhere by the authors, were used to reveal the solidification microstructure and macrostructure. The results allow a new solidification model to be proposed, where each solidification unit is a grain of eutectic austenite that has a dendritic substructure and contains a very large number of graphite nodules. A pattern of microsegregation exists inside each solidification grain, while no intergranular microsegregation has been detected. A procedure to characterise the solidification refinement was developed considering the location of the last to freeze areas. **MST/5169**

The authors are in the Metallurgy Division INTEMA, National University of Mar del Plata (CONICET), B7608FDQ Mar del Plata, Argentina (jsikora@fi.mdp.edu.ar). *Manuscript received 25 July 2001; accepted 4 October 2001.*

List of symbols and abbreviations

A_{cell}	average area per cell
A_{grain}	average area of eutectic grains
A_{nodule}	average nodule area
DAAS	direct austempering after solidification
DI	ductile cast iron
LTF	last to freeze
MA, MI1, MI2	melts
MN	multinodular
N_c	average number of cells per unit area
$N_{c,V}$	number of cells per unit volume
N_{grain}	average number of grains per unit area
$N_{g,V}$	number of grains per unit volume
N_n	average number of nodules per unit area
$N_{n,c}$	average number of nodules per cell
$N_{n,grain}$	average number of nodules per grain
$N_{n,g,V}$	number of nodules per grain in volume
$N_{n,V}$	number of nodules per unit volume
UN	uninodular

Introduction

Ductile cast irons are materials of great technological importance that are used in the construction of a large number of components. Despite their extensive application, there are still a number of aspects of their metallurgy that are not thoroughly understood. In particular, significant research efforts have been carried out to understand the solidification of these alloys and the resulting microsegregation, aiming to reach a better control of their microstructure and mechanical properties.

The literature shows two major physical models to explain eutectic DI solidification. Most solidification experts agree today that the solidification of eutectic DI involves the formation of austenite dendrites and graphite nodules or spheroids. The interaction of the growing austenite with the nodules originate solidification units, described as engrossed austenite dendrites, which contain several graphite nodules,[1,2] as shown schematically in Fig. 1. This will be referred to as the MN model. On the other hand, other researchers, mostly involved with the modelling of microstructure and microsegregation, use an earlier solidification model in which solidification units are formed by graphite nodules enveloped by austenite shells, as shown in Fig. 2.[3–7] This will be referred to as the UN model. The discrepancies regarding the solidification of DI are difficult to resolve because, after solidification is complete, solid state transformations take place during cooling to room temperature, making it impossible to reveal the solidification structure by standard metallographic techniques. As a consequence, the standard characterisation of DI structures includes only the description of the matrix microstructure at room temperature and the graphite count and morphology. The coarsening of the structure as the solidification rate decreases is characterised indirectly by the coarsening of the graphite nodules. There is no method based on the observation of the true solidification structure of the matrix.

In recent publications, the authors reported the development of novel methods to reveal micro- and macroscopically the solidification structure of near eutectic DI cast in sand moulds.[8–10] The evidence obtained through the use of these methods contradicted the previous solidification models, described above, and led the authors to propose a new explanation of the solidification mechanism of eutectic DI. According to this explanation,[10] the solidification begins with the independent nucleation of graphite and austenite in the melt. The austenite grows dendritically, trapping and enveloping graphite nodules as they collide with the dendrites. Further graphite growth requires the diffusion of C to the nodules through the austenite envelope. The macrographic technique developed by Boeri and Sikora[10] showed that each solidification unit is formed by a large austenite dendrite that contains many graphite nodules. It has been shown that small departures from the eutectic composition do not markedly affect the solidification process.[11] Earlier experimental results and existing models must be critically reviewed and compared with this new solidification model.

The objectives of this study are to make a detailed analysis of old and new solidification models, and to develop a procedure to characterise the solidification structure of near eutectic DI cast in sand moulds.

Experimental procedure

MATERIALS

Ductile iron melts used were of near eutectic composition, and were produced in commercial foundries and pilot plants using medium frequency induction furnaces. Charge materials were DI quality pig iron (low P, S, and Mn), low C steel scrap, foundry returns, ferroalloys, electrolytic Ni and Cu, and graphite. The melt was nodularised by using 2 wt-% of Fe–Si–Mg–Ca–Ce (9 wt-%Mg), and post-inoculated with 0·5 wt-% of Fe–Si (75 wt-%Si).

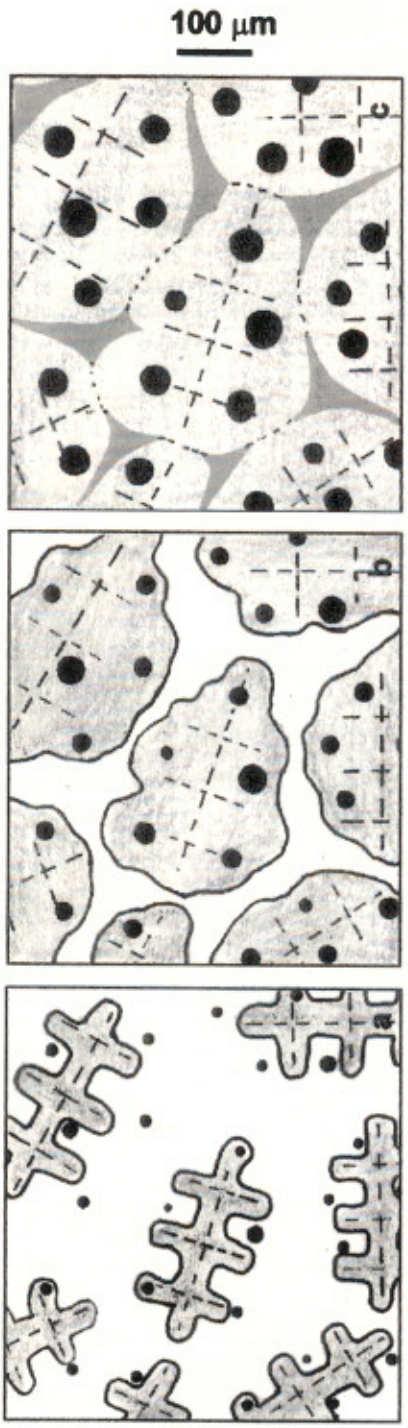

1 Schematic of sequence of solidification of eutectic ductile cast iron according to multinodular model: black lines represent boundary between solidification units; dark grey zones at which three solidification units meet correspond to last to freeze areas in melt

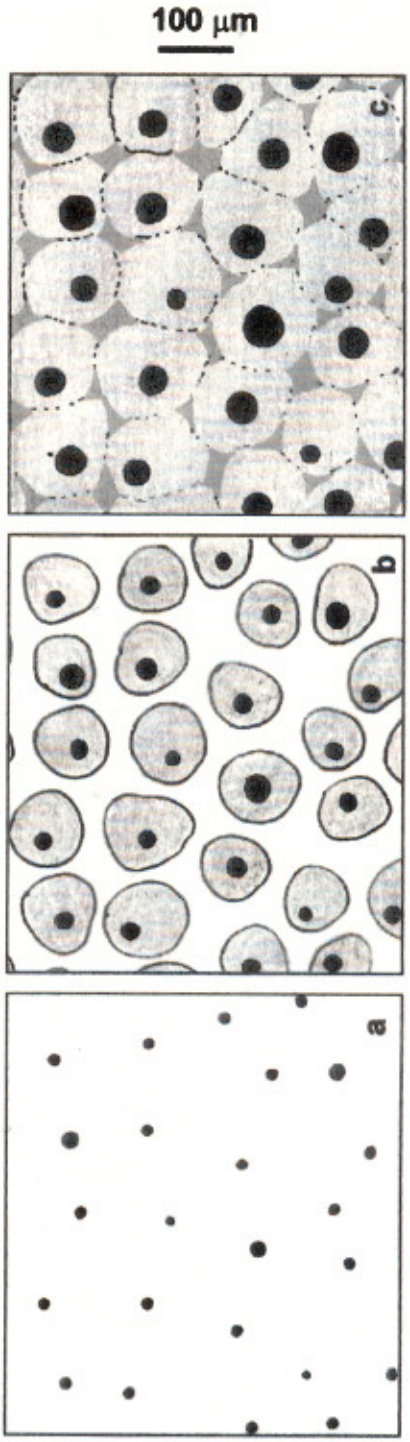

2 Schematic of sequence of solidification of eutectic ductile cast iron according to uninodular model: black lines represent boundary between solidification units; dark grey zones at which three solidification units meet correspond to last to freeze melt

Table 1 lists the chemical composition and the graphite characteristics (ASTM A247)[12] of the melts used.

The Y blocks of 13, 25, and 75 mm (ASTM A395),[13] and round bars of 20 mm diameter and 100 mm long, were cast in resin bonded sand moulds. Metallographic samples were obtained from the Y blocks and round bars at the locations shown schematically in Fig. 3.

METALLOGRAPHIC STUDY

The metallographic techniques used in this study were developed elsewhere by the authors.

Micrographic technique

The technique reveals the solidification microstructure through the use of a reagent that brings up the microsegregation patterns generated during solidification, as reported by Rivera *et al.*[8] For better results, it is recommended to carry out a ferritisation anneal on the samples before etching. In this study, the etching procedure was applied on samples taken from Y blocks. Typical results are shown in black and white in Fig. 4*a**. The light patches

*Colour versions of all micrographs, which provide enhanced information on the microstructures, are available from the authors.

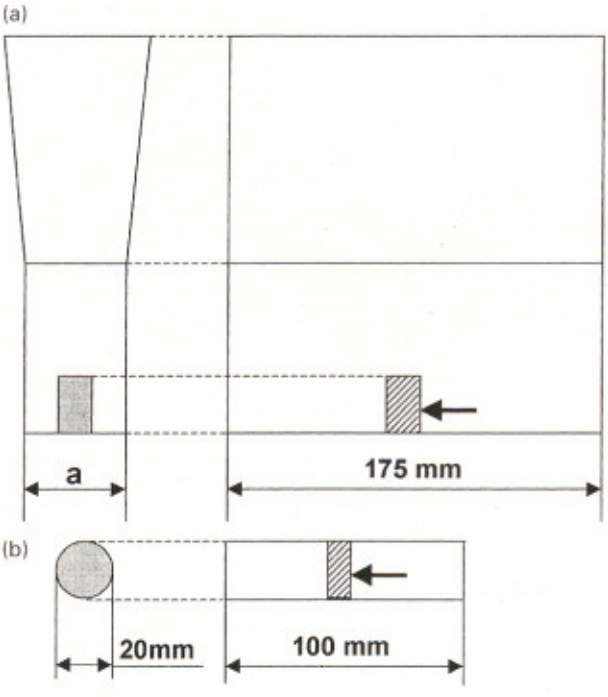

a Y blocks; *b* round bars

3 Experimental castings: arrows show location of samples used for metallographic characterisation: *a*=13, 25, and 75 mm

(arrowed) surround and make it possible to identify the location of the microsegregated regions corresponding to the LTF melt. To characterise the distribution of such regions, a procedure was developed as described below. On a ×100 micrograph of the colour etched samples, lines are manually drawn between the location of neighbouring LTF regions (Fig. 4*b*). This defines a pattern of closed regions, that have been referred to as 'cells' in the past and were considered to be the solidification units.[14] Such nomenclature is still used in the present article, although it must be pointed out that, under the current understanding of the authors, the division into cells does not have physical meaning, but is only a means to characterise the dispersion of LTF.

On each sample analysed, at least 50 cells were identified and the average number of nodules per cell $N_{n,c}$ was measured. The number of nodules per unit area N_n and the average nodule area A_{nodule} were also measured on each sample, and the number of cells per unit area N_c was calculated as the ratio between N_n and $N_{n,c}$. The average area per cell A_{cell} was calculated as N_c^{-1}.

Macrographic technique

The observation of the macrostructure requires DAAS[10] to be carried out. In this process, the cast parts are shaken out from the mould when their temperature is ~950°C, and

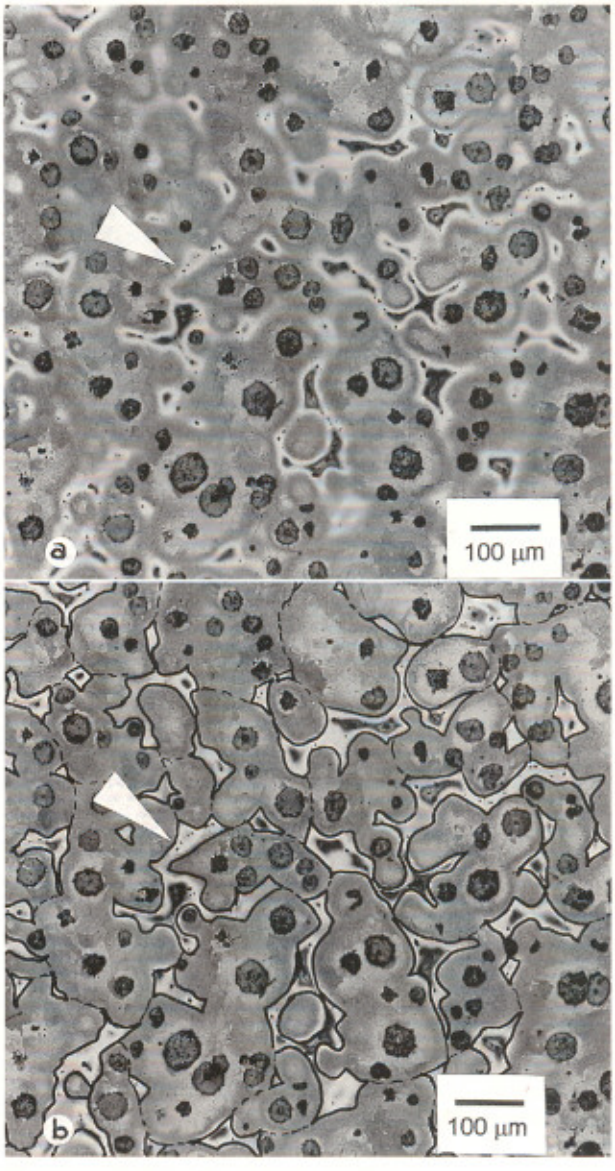

4 *a* black and white print of melt MI1 after colour etching and *b* same area as *a* with LTF zones and cell contour marked manually

transferred to a furnace held at 900°C, where they remain for 30 min to allow temperature stabilisation. The parts are then austempered in a molten salt bath held at 360°C, for 90 min. After DAAS treatment, the matrix microstructure of the samples shows a fine mixture of ferrite needles and retained austenite, typical of austempered ductile iron. The retained austenite retains the crystalline orientation defined during solidification. Therefore, later etching with Picral (5 wt-%) reveals the grain structure of the eutectic

Table 1 Chemical composition and characterisation of graphite phase*

	Chemical composition, wt-%										Graphite characteristics		
Melt	Fe	C	Si	Mn	Cu	Ni	Cr	Mo	Mg	Cast size, mm	N_L, %	N_S	N_n, nodules mm^{-2}
MA	Bal.	3·00	3·10	0·27	0·87	0·74	...	...	0·060	Bar ϕ=20	100	6/7	291
MI1	Bal.	3·50	2·09	0·80	0·83	...	0·26	...	0·027	Y block=13	100	5/6	253
										Y block=25	100	5/6	200
										Y block=75	90	5	78
MI2	Bal.	3·20	2·95	0·22	1·00	0·71	...	0·20	0·056	Y block=13	100	6/7	348
										Y block=25	100	6	225
										Y block=75	100	5	120

*N_L nodularity; N_S nodule size; N_n nodule count.

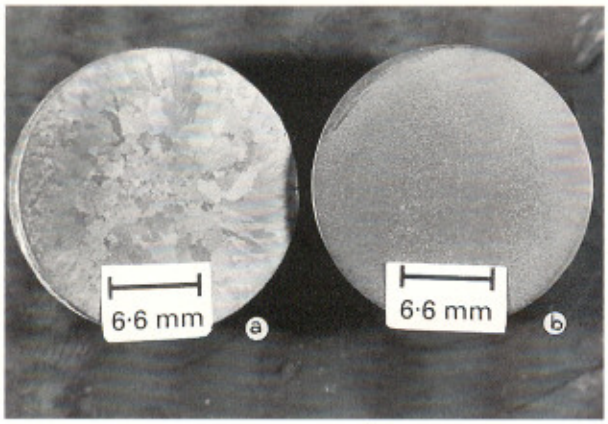

a direct austempering after solidification; *b* conventional austempering

5 Macrographs of melt MA etched with 5 wt-% Picral

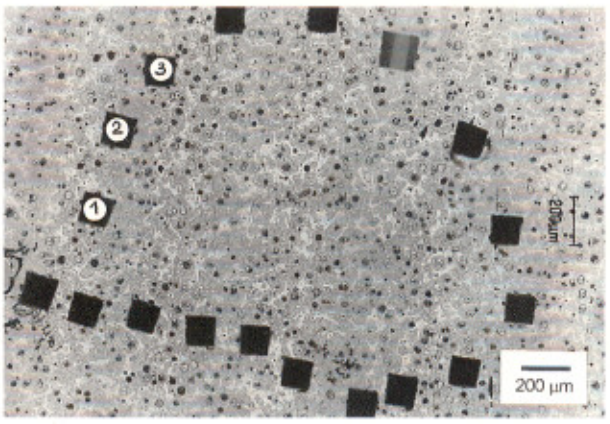

6 Micrograph of melt MA after direct austempering after solidification procedure and colour etching: hardness indentations show position of grain boundary of eutectic austenite

austenite. This procedure was carried out on samples taken from round bars. Figure 5*a* shows the result of the etching of a sample of melt MA, obtained using the DAAS technique. Figure 5*b* shows the results of the etching of another sample of the same melt cast without the use of DAAS, and austempered using the same temperature and time as the sample of Fig. 5*a*. It is very clear that DAAS allows the macrostructure to be revealed, while no evidence of such a structure is present in samples cooled down conventionally after solidification.

The result shown in Fig. 5*a* is typical for all DIs investigated. It shows a grain structure similar to that found in cast parts of most metallic alloys. The average area of the eutectic grains A_{grain} was measured. The number of grains per unit area N_{grain} was calculated as A_{grain}^{-1}, and the number of nodules per grain $N_{n,grain}$ was calculated as the product of N_n and A_{grain}.

Results and discussion

ANALYSIS OF VALIDITY OF EARLIER SOLIDIFICATION MODELS

Uninodular model

The progress of the solidification according to the UN model, shown schematically in Fig. 2, would lead to a distribution of the microsegregation as that shown schematically in Fig. 2*c*, where if it is assumed, for example, that the average nodule diameter is 40 µm and the average distance between nodules is 120 µm (approximate values for a 25 mm thick plate cast in a sand mould), typical distances between microsegregated (LTF) regions would be similar to the average distance between nodules. The actual distribution of microsegregation, shown in Fig. 4*a*, is significantly different from what is predicted by the UN model. Note that the average nodule size of the sample of Fig. 4*a* is ~40 µm, similar to what has been assumed in the schematic of Fig. 2*c*. The actual distance between LTF is about three times larger than that predicted by the UN model. If this ratio is taken to a three-dimensional space, it would mean that the UN model predicts a dispersion of the microsegregation regions about 27 times larger than that actually observed. This indicates that the UN model fails to predict the microsegregation pattern. Moreover, an even more negative fact is found when the predictions of the UN model are compared with the macrostructure shown in Fig. 5, where the grain volume is about three orders of magnitude greater than that of the UN model. It must be pointed out that a large number of mathematical models of microsegregation and solidification of DI are based on the UN model.[3–7]

Multinodular model

The progress of the solidification according to the MN model would lead to the distribution of the microsegregation shown schematically in Fig. 1*c*. This is in good coincidence with the actual pattern, shown in Fig. 4*a*. This is not surprising, since the MN model has been developed through the observation of the microsegregation patterns.[8] The MN model proposes that areas between microsegregated regions are the actual eutectic solidification units. Nevertheless, the size reported for such units is much smaller than that revealed by macrography (Fig. 5). Moreover, according to the MN model the microsegregation inside each solidification unit is very small. Therefore, it is advisable to examine simultaneously the micro- and macrostructure. In order to examine the microstructure while keeping track of the macrostructure, the location of a grain boundary revealed by macroetching was marked by Vickers hardness indentations. The same sample was repolished and colour etched, as shown in Figs. 6 and 7 (in higher magnification). Noticeably, no predominant microsegregation is seen at the boundary between solidification units, but extensive microsegregation is observed inside each solidification unit. This points out the inadequacy of the MN model, and the need to formulate a new approach.

PROPOSED OF IMPROVEMENT TO NEW SOLIDIFICATION MODEL

The model proposed by Boeri and Sikora[10] agrees with most of the experimental evidences, but can still be improved to account for the distribution of the microsegregation

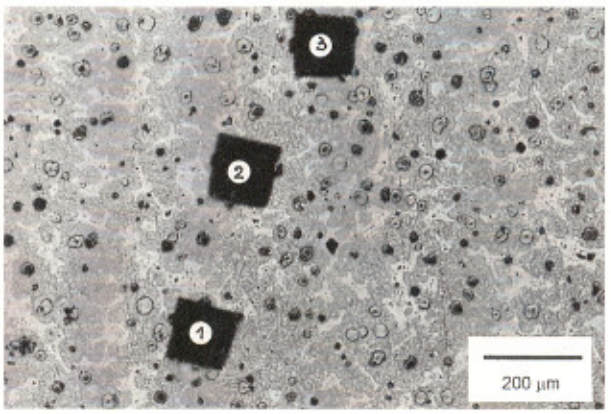

7 Micrograph of same sample as Fig. 6 at higher magnification

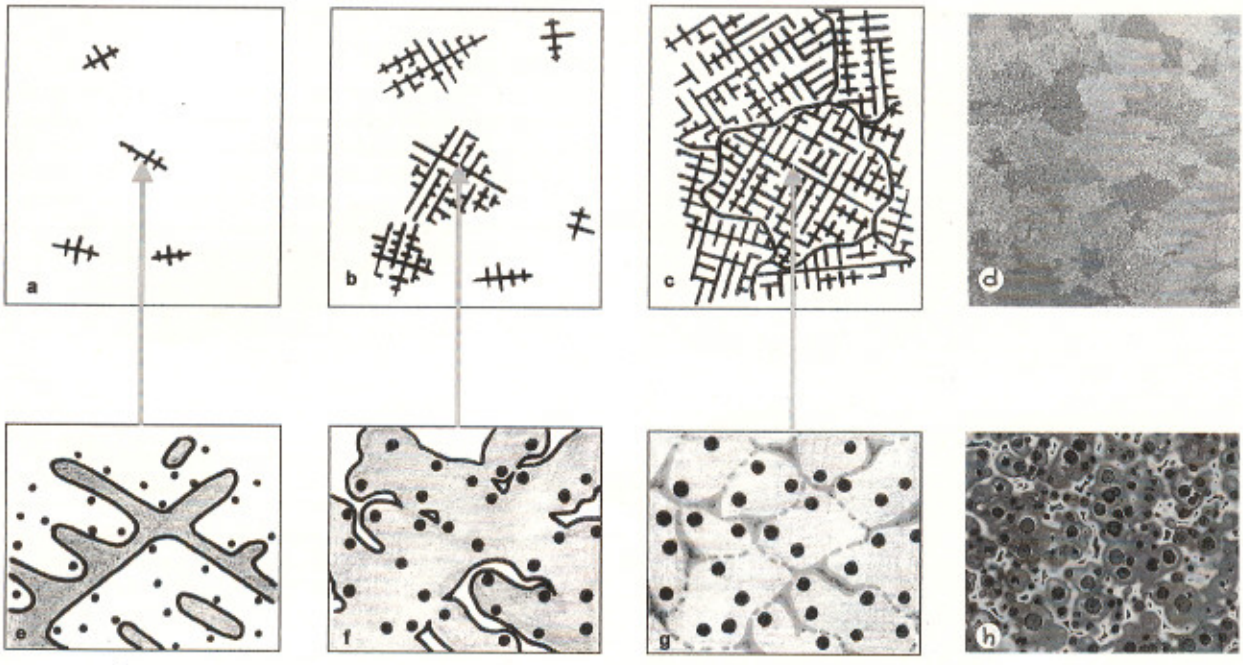

a–c solidification macrostructure (equiaxed grains); *d* actual macrostructure; *e–g* solidification microstructure; *h* actual microstructure

8 Schematic illustration of sequence of solidification of eutectic ductile cast iron

in better detail. A new version of this model is proposed here, as shown schematically in Fig. 8. Figure 8*a–c* represent different stages of the formation of the macrostructure. The growth of austenite dendrites that originate the grains is shown. In this sequence, the presence of graphite nodules is ignored, since the size of the graphite particles is too small at this scale. Figure 8*e–g* represent a higher magnification view of the stages corresponding to Fig. 8*a–c* respectively, where the nature of the interaction of austenite dendrites and graphite nodules is portrayed. According to the model, the solidification of eutectic DI begins with the independent nucleation and growth of austenite and graphite from the melt, with the austenite growing dendritically, as shown in Fig. 8*a* and *e*. As the solid fraction increases, the austenite dendrites grow (Fig. 8*b*) and they contact and envelop most of the graphite nodules, as shown in Fig. 8*f*. Further growth of enveloped nodules is controlled by the diffusion of C from the liquid to the nodules, through the austenite. The advance of the austenite dendrites leaves significant amounts of melt between the secondary arms. In this manner, at the point at which growing dendrites interact, defining the grain size, there is still a large fraction of melt inside each grain. The structure after solidification is complete is represented in Fig. 8*c* and *g*. Figure 8*c* shows the dendritic substructure of the eutectic austenite grains. The dark grey regions of Fig. 8*g* represent the location of the LTF areas that can be revealed by colour etching. The dotted lines, manually drawn between the location of neighbouring LTF regions, define the closed regions called 'cells'.

According to this explanation of the solidification process of eutectic DI, the solidification unit is the grain of eutectic austenite that has a dendritic structure and contains a large number of graphite nodules and several 'cells'. A pattern of microsegregation exists inside each austenite grain.

CHARACTERISATION OF SOLIDIFICATION STRUCTURE

Having developed micro- and macrographic techniques to reveal the solidification structure of DI, it is now possible to characterise it in detail. For example, the characterisation of the macrostructure of melt MA is: $A_{grain} = 1{\cdot}8$ mm^2; $N_{grain} = 0{\cdot}6$ grains mm^{-2}; and $N_{n.grain} = 524$ nodules grain^{-1}. Note that the average grain size is relatively large. The DAAS technique is certainly useful for research, since it allows the observation of features that were earlier ignored. Nevertheless, it is also certain that this technique cannot be applied on samples obtained from regular foundry products, therefore it is not useful for characterising the solidification structure of such products. The micrographic technique, on the other hand, can be applied on every DI sample. Colour etching reveals the location of LTF. According to the solidification model introduced recently, the size of the regions lying between LTF is related to the dendrite secondary arm spacing. This spacing is a parameter usually measured to evaluate the influence of the cooling rate on the refinement of the dendritic structure.[15] Therefore, the cell count N_c, determined by the procedure described in the experimental methods section, is closely related to the degree of refinement of the austenite in DI, and will be used to characterise it. The refinement of the graphite is properly characterised by the parameter N_n.

Figure 9 shows black and white prints of micrographs of samples of melt MI2 obtained from Y blocks of 13 and 75 mm thickness, after ferritisation and colour etching. The coarsening of the austenite dendritic structure caused by the increase in solidification time is seen clearly in Fig. 9*b*, where the LTF regions are larger and lie farther apart than in Fig. 9*a*. The coarsening of the graphite nodules is also evident, as they become larger and the nodule count diminishes as the section size increases.

Table 2 lists values of N_n, $N_{n,c}$, and N_c for melts MI1 and MI2 cast in different sections. The results show that as the section size increases, the number of nodules per cell $N_{n,c}$ increases, and the cell count N_c diminishes more markedly than the nodular count N_n. This is seen in detail in Table 3, which lists the percent of reduction of N_n and N_c as the section size increases.

STEREOLOGIC CHARACTERISATION

In order to advance in the characterisation of the solidification units of eutectic DI, it seems relevant to perform some calculations to describe the size of the features in volumetric terms. The number of nodules per unit volume

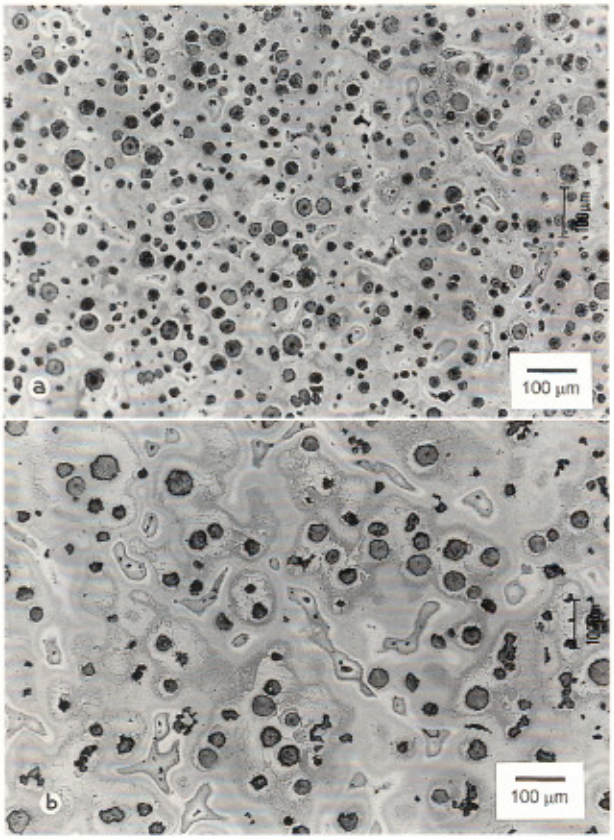

a 13 mm; *b* 75 mm

9 Black and white micrographs of different Y blocks of melt MI2 after colour etching

Table 2 Metallographic characterisation of different sections*

Melt	Section size, mm	Metallographic parameters		
		N_n, nodules mm^{-2}	$N_{n,c}$, nodules cell^{-1}	N_c, cell mm^{-2}
MI1	13	253	6·0	42
	25	200	7·8	25
	75	78	11·2	7
MI2	13	348	8·3	42
	25	225	10·5	21
	75	120	20·4	6

*Nodule count N_n; nodules per cell N_{nc}; cell count N_c.

Table 3 Reduction of nodule count N_n and cell count N_c as the section size increases, %

Melt	Increase from 13 to 25 mm		Increase from 25 to 75 mm	
	N_n	N_c	N_n	N_c
MI1	−21	−40	−61	−72
MI2	−35	−50	−46	−71

N_{nV} can be estimated by using Hilliard's equation[16]

$$\bar{A}_A(z) = [A(z)/L^2] = V/L^3 \quad (1)$$

where L is the length of the test plane, $A(z)$ is the area of intersection of a particular test plane with the graphite phase, $A_A(z)$ is the fraction of the area of the test plane that is occupied by the graphite phase, $\bar{A}_A(z)$ is the expected value of $A_A(z)$, averaged over the domain of axis z (that is, all positions of test planes in the structure), and V/L^3 is the volume fraction occupied by the graphite phase.
Assuming

$$\bar{A}_A(z) = N_n . A_{nodule} \quad (2)$$

and

$$V/L^3 = N_{n,V} . V_{nodule} \quad (3)$$

where A_{nodule} is the average nodule area and V_{nodule} is the average nodule volume. Equating equations (2) and (3)

$$N_{n,V} = N_n . (A_{nodule}/V_{nodule}) \quad (4)$$

Assuming that cells and grains are spherical and have a radius r, the number of cells per unit volume $N_{c,V}$, and the number of grains per unit volume $N_{g,V}$, can be calculated as follows

$$r_{cell} = (A_{cell}/\pi)^{1/2} \Rightarrow V_{cell} = (4/3)\pi r_{cell}^3 \Rightarrow N_{c,V} = V_{cell}^{-1} \quad (5)$$

$$r_{grain} = (A_{grain}/\pi)^{1/2} \Rightarrow V_{grain} = (4/3)\pi r_{grain}^3$$

$$\Rightarrow N_{g,V} = V_{grain}^{-1} \quad (6)$$

The number of nodules per cell in volume $N_{n,c,V}$, and the number of nodules per grain in volume $N_{n,g,V}$, can be calculated as

$$N_{n,c,V} = N_{n,V} V_{cell} \quad (7)$$

$$N_{n,g,V} = N_{n,V} V_{grain} \quad (8)$$

The results of the stereologic characterisation of melt MA are listed in Table 4. It is important to note that, for the samples investigated, each eutectic grain contains approximately 18000 nodules and 400 cells. This is very far from the single nodule inside each grain assumed by the UN model, and also far from the few nodules assumed by the MN model.

Future work

Future efforts will be aimed at identifying the influence of the cooling rate and the equivalent carbon content on the coarseness of the solidification structure of DI. The relationship between the refinement of the solidification grain size and the refinement of the microsegregation pattern will be also investigated.

Conclusions

1. The knowledge about the solidification structure of ductile cast iron gained through the use of recently developed micro- and macrographic techniques, has led to the proposal of a new solidification model, in which eutectic

Table 4 Stereological characterisation of melt MA*

Microstructural parameters				Macrostructural parameters			
$N_{n,V}$, nodules mm^{-3}	$N_{c,V}$, cells mm^{-3}	Nodules per cell volume	V_{cell}, mm^3	$N_{g,V}$, grains mm^{-3}	Nodules per grain volume	Cells per grain volume	V_{grain}, mm^3
23557	47	503	$1{\cdot}99 \times 10^{-3}$	1·3	18375	392	$7{\cdot}8 \times 10^{-1}$

*$N_{n,V}$ nodules per unit volume; $N_{c,V}$ cells per unit volume; V_{cell} average cell volume; $N_{g,V}$ grains per unit volume; V_{grain} average grains volume.

solidification units or grains are large austenite dendrites that contain a very large number of graphite nodules.

2. The inadequacy of the earlier solidification models has been demonstrated.

3. The microsegregation of the alloying elements, resulting from solidification, takes place intradendritically while interdendritic or intergranular microsegregation is not evident.

4. The degree of refinement of the solidification austenite structure can be assessed by the cell count N_c value.

5. Under the present experimental conditions, the average size of equiaxed solidification units measured on near eutectic 20 mm round bars cast in sand moulds, is approximately 1·2 mm in diameter and 0·8 mm^3 in volume. Units of this size contain ~18 000 graphite nodules.

References

1. R. BOERI and F. WEINBERG: *AFS Trans.*, 1989, **97**, 179–184.
2. D. BANERJEE and D. STEFANESCU: *AFS Trans.*, 1991, **99**, 747–759.
3. E. FRAS, W. KAPTURKIEWICZ, and A. BURBIELKO: in 'Physical metallurgy of cast iron V: advanced materials research', (ed. G. Lesoult and J. Lacaze), 499–504; 1997, Swizerland, Scitec.
4. CH. CHARBON and M. RAPPAZ: in 'Physical metallurgy of cast iron V: advanced materials research', (ed. G. Lesoult and J. Lacaze), 453–460; 1997, Swizerland, Scitec.
5. L. LIU and R. ELLIOTT: *Int. J. Cast Met. Res.*, 1998, **10**, 301–305.
6. L. LIU and R. ELLIOTT: *Int. J. Cast Met. Res.*, 1999, **12**, 75–82.
7. B. LIU: *Int. J. Cast Met. Res.*, 1999, **11**, 259–266.
8. G. RIVERA, R. BOERI, and J. SIKORA: *Cast Met.*, 1995, **8**, 1–5.
9. J. MASSONE, R. BOERI, and J. SIKORA: *Int. J. Cast Met. Res.*, 1999, **11**, 419–424.
10. R. BOERI and J. SIKORA: *Int. J. Cast Met. Res.*, 2001, **13**, 307–313.
11. G. RIVERA: 'Solidification structure of SG cast iron', Doctoral thesis, National University of Mar del Plata, Argentina, 2000.
12. Standard A247, ASTM, Philadelphia, PA, 1978.
13. Standard A395, ASTM, Philadelphia, PA, 1956.
14. G. RIVERA, R. BOERI, and J. SIKORA: in 'Physical metallurgy of cast iron V: advanced materials research', (ed. G. Lesoult and J. Lacaze), 169–174; 1997, Switzerland, Scitec.
15. M. FLEMINGS: 'Solidification processing'; 1974, New York, NY, McGraw–Hill.
16. J. HILLIARD: 'Quantitative microscopy', chapter 3; 1968, New York, NY, McGraw–Hill.